JACS
JOURNAL OF THE AMERICAN CHEMICAL SOCIETY
Communication
pubs.acs.org/JACS

A 3.6 nm Ti_{52}–Oxo Nanocluster with Precise Atomic Structure

Wei-Hui Fang, Lei Zhang,* and Jian Zhang*

State Key Laboratory of Structural Chemistry, Fujian Institute of Research on the Structure of Matter, Chinese Academy of Sciences, Fuzhou, Fujian 350002, P. R. China

Supporting Information

ABSTRACT: We report a 3.6 nm Ti_{52}–oxo cluster with precise atomic structure, which presents a largest size record in the family of titanium–oxo clusters (TOCs). The crystal growth of such large Ti_{52} is based on a stepwise interlayer assembly approach from Ti_6 substructures. The possible growth mechanism of Ti_{52} could be deduced from crystal structures of two substructures, Ti_6 and Ti_{17}, which were also synthesized under similar conditions as Ti_{52}. Moreover, these TOCs show cluster-size-dependent photocatalytic hydrogen evolution activities with Ti_{52} giving a H_2 production rate up to 398 μmol/h/g, which is also the highest record in the family of TOCs. This work not only represents a milestone in constructing large TOCs with comparable sizes as TiO_2 nanoparticles but also brings significant advances in improving photocatalytic behaviors of TOCs.

Solar energy driven water splitting has become a promising way for the clean and sustainable production of hydrogen and will provide a practicable solution to the global energy and environment crisis.[1−3] Titanium dioxide (TiO_2) and related Ti–O nanomaterials are the most widely applied catalytic materials for water splitting due to their low cost, high activity, and environment-friendly characteristics.[4−8] Size, composition, and atomic connectivity are important factors that determine the physical behaviors of titanium oxide nanoparticles.[9,10] To build structure–property relationship and achieve chemical fine-tuning, understanding the binding modes and electronic structures of Ti–O materials at the molecular level is crucial.[11,12]

Since the first crystal structure of the initial crystalline hydrolysis product of titanium tetraethoxide was determined by X-ray diffraction in 1967,[13] tremendous progress has been made on the research on crystalline titanium–oxo clusters (TOCs).[9,10,14−16] Their crystalline phases offer the opportunity to get accurate structural information, providing a unique bridge between theoretical modeling, crystallography, and spectroscopy.[17,18] However, despite lots of TOCs have been characterized, the assembly of crystalline high-nuclearity TOCs with comparable sizes as TiO_2 nanoparticles has always been a challenge. The most majority of the reported TOCs show nuclearities less than 42 titanium atoms and core diameters smaller than 1.5 nm (Figure 1).[12,14,19−27] Moreover, although most of the driving forces of the research on TOCs come from simulating the photocatalytic titanium oxide materials, the studies on their photocatalytic H_2 evolution applications still remain very rare.[28,29]

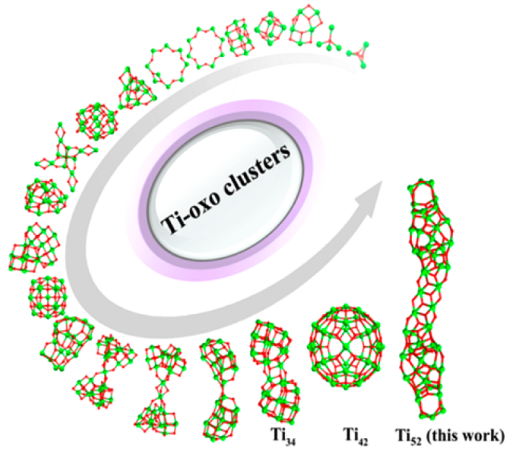

Figure 1. Illustration of the development of the TOCs family.

In this work, we set a new record for the family of TOCs and report a 3.6 nm TOC with precise atomic structure. Through controlling the chelating ligands and reactants concentrations, we successfully achieve the stepwise assembly from $Ti_6(\mu_3\text{-}O)_4(BDC)_2(PA)_2(OiPr)_{10}$ (**COM-1**; BDC = 1,2-benzenedicarboxylate; HPA = propionic acid, **COM** denotes cluster–organic material), via $Ti_{17}(\mu_2\text{-}O)_2(\mu_3\text{-}O)_{18}(\mu_4\text{-}O)_2(PA)_8(OiPr)_{16}$ (**COM-2**) toward $Ti_{52}(\mu\text{-}OH)_2(\mu\text{-}O)_{14}(\mu_3\text{-}O)_{50}(\mu_4\text{-}O)_8(PA)_{34}(OiPr)_{28}$ (**COM-3**), whose core skeleton diameters span from 0.9 to 3.6 nm. All of these **COMs** represent layered structures with both **COM-2** and **COM-3** being constructed from the basic $\{Ti_6\}$ unit in **COM-1**. To the best of our knowledge, **COM-3** is the largest titanium–oxo cluster reported to date. Its $\{Ti_{52}O_{74}\}$ cluster core can even be directly visualized by high-resolution transmission electron microscope (TEM) analysis. Moreover, photocatalytic H_2 evolution studies indicate cluster-size dependent activities, with **COM-1** and **COM-3** displaying H_2 production rate of 206 and 398 μmol/h/g, respectively. Cycling tests have confirmed the high photocatalytic stabilities of **COM-1** and **COM-3**.

The crystal growth of such a large Ti–O cluster as **COM-3** is quite challenging, and it is possibly based on a stepwise interlayer assembly approach from Ti_6 substructures. Fortunately, two substructures (**COM-1** and **COM-2**) were also obtained under similar synthetic conditions as **COM-3**, so that the growth mechanism could be deduced. The solvothermal reaction of $Ti(OiPr)_4$ with 1,2-benzenedicarboxylic acid in the presence of propionic acid in isopropanol at 80 °C for 72 h

Received: April 5, 2016
Published: June 1, 2016

DOI: 10.1021/jacs.6b03489
J. Am. Chem. Soc. 2016, 138, 7480–7483

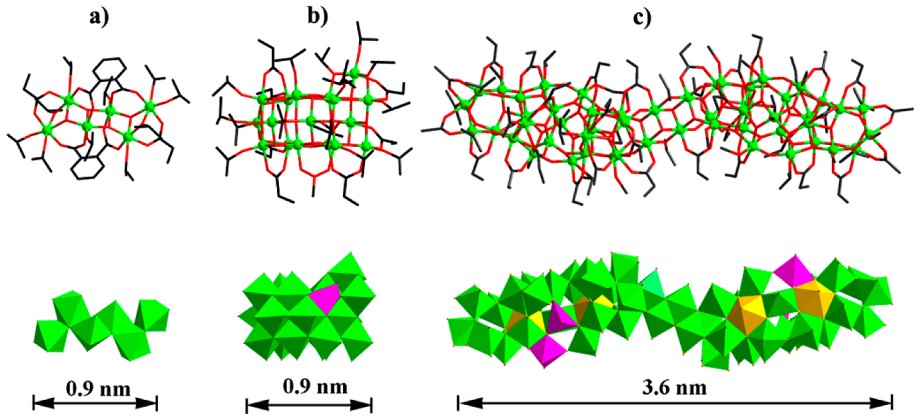

Figure 2. Crystal structures of **COM-1** (a), **COM-2** (b), and **COM-3** (c). The above array displays their molecular structures. The below array represents the polyhedral drawing of the $\{Ti_6\}$, $\{Ti_{17}\}$, and $\{Ti_{52}\}$ clusters, with their core diameters highlighted. H and C atoms have been omitted for clarity. Atom color code: green Ti; red O; black C. Polyhedral color code: pink TiO_5; green TiO_6; yellow TiO_7.

gave rise to colorless crystals of **COM-1** after cooling to room temperature. Single-crystal X-ray diffraction analysis indicated that **COM-1** contained a ribbon-like $\{Ti_6(\mu_3\text{-}O)_4\}$ unit whose two sides were blocked off by two BDC molecules (Figure 2a). It would be rational that if these two BDC ligands were taken away, more Ti_xO_y species could be attached to the two sides of **COM-1** to give "thicker" and larger clusters. Indeed, upon removing BDC ligands from the reaction system, colorless crystals of **COM-2** were formed whose structure comprised two $\{Ti_6(\mu_3\text{-}O)_4\}$ subunits connected by some isolated Ti atoms (Figure 2b). More interestingly, when further doubling concentration of the reactions, the largest **COM-3** was obtained, which contained greatly expanded sublayers (Figure 2c). It should be noted that the yield of **COM-2** was quite low, indicating that it might be the intermediate product between the $\{Ti_6(\mu_3\text{-}O)_4\}$ basis layer and **COM-3**.

The synthetic and structural evolution between the above three COMs is illustrated in Figure 3. Like taking a flake of

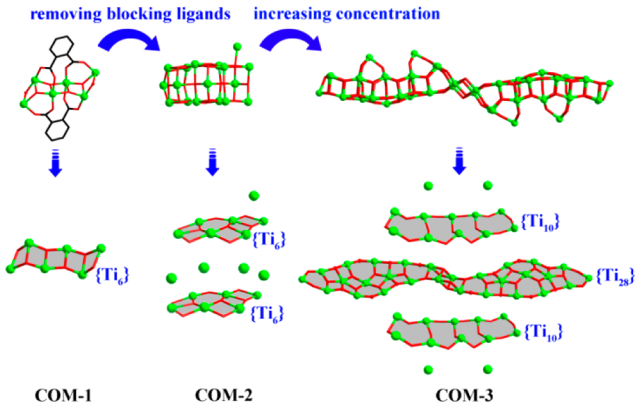

Figure 3. Synthetic and structural evolution between $\{Ti_6\}$ in **COM-1**, $\{Ti_{17}\}$ in **COM-2**, and $\{Ti_{52}\}$ in **COM-3**. The $\{Ti_6\}$ flakes in **COM-1** and **COM-2** and the $\{Ti_{10}\}$ and $\{Ti_{28}\}$ sublayers in **COM-3** are highlighted in gray filling. Atom color code: green Ti; red O; black C.

carbon with a thickness of just one atom to form the two-dimensional material graphene, the structures of these COMs can also be associated with peeling the onions. The belt-like $\{Ti_6\}$ core fastened by four μ_3-O bridges in **COM-1** represents the simplest Ti−O flake fragment of such cluster series. However, the BDC ligands located above and below this flake make it unable to be further extended. Naturally, when the blocking BDC ligands are eliminated, the obtained structure of **COM-2** comprises two parallel Ti_6 flakes stuffed with four Ti atoms plus an apical one. Moreover, in the $\{Ti_6\}$ core of **COM-1** the two Ti_3O units are twisted; while in the $\{Ti_6\}$ flake of **COM-2** they are almost on the same plane, making it easier to incorporate more Ti atoms to give expansive layers. Such deduction has successfully been verified by the structure of **COM-3**, which is prepared by simply increasing the titanium concentration. To better interpret the structure of **COM-3**, the $\{Ti_{52}\}$ giant cluster can be divided into one central $\{Ti_{28}\}$ layer, two $\{Ti_{10}\}$ ladders decorated from two sides, and four apical Ti atoms. Both the $\{Ti_{28}\}$ and $\{Ti_{10}\}$ sublayers should be generated from the basic $\{Ti_6\}$ flakes by adding/moving some μ_3-O bridges to adapt the requirements of Ti attaching for structure growth. Therefore, by removing blocking BDC ligands, two $\{Ti_6\}$ flakes in **COM-1** can be held together to form **COM-2**; further incorporating more Ti atoms to these $\{Ti_6\}$ flakes can give rise to the $\{Ti_{28}\}$ layer and $\{Ti_{10}\}$ ladder in **COM-3**. Such structural evolution can also be supported by electrospray-ionization mass spectrometry (ESI−MS) analysis (Figures S27 to S30). The fingerprint peaks of $\{Ti_6\}$ species are presented in the spectra of the synthetic reactions for all clusters, indicating that it could be the cornerstone for the assembly toward $\{Ti_{17}\}$ and $\{Ti_{52}\}$.

COM-3 is currently the largest TOC protected by surface organic ligands. The crystal structure of **COM-3** represents a centrosymmetric $\{Ti_{52}\}$ core built from two symmetry-related boat-like $\{Ti_{26}\}$ subarchitectures (Figure S19). The outer face of this $\{Ti_{52}O_{74}\}$ nanorod is functionalized by 34 PA ligands and 28 isopropyl molecules. In contrast to the exclusively existed 6-coordinated Ti ions and μ_3-O centers in the TiO_2 nanoparticles, the nanocluster of **COM-3** shows a significant structural diversity. There are four 5-coordinated (Ti1, Ti5), four 7-coordinated (Ti4, Ti11), and 44 6-coordinated (Ti2, Ti3, Ti6−Ti10, Ti12−Ti26) titanium ions. The 52 Ti atoms are then interconnected through three different kinds of oxo bridges: 16 μ-O(H), 50 μ_3-O, and 8 μ_4-O. Each of the 34 PA ligands bridges two adjacent Ti atoms in a $(\kappa^1\text{-}\kappa^1)\text{-}\mu$-coordination mode. Two of the 28 isopropyl ligands act as bridges between the two $\{Ti_{26}\}$ subunits, and the others act as terminal ligands. The $\{Ti_{26}\}$ subunit can also seem to be a layered structure consisting of a $\{Ti_{14}\}$ bottom layer, a $\{Ti_{10}\}$ middle layer, and two decorated titanium vertexes. Remarkably,

DOI: 10.1021/jacs.6b03489
J. Am. Chem. Soc. 2016, 138, 7480−7483

in the $\{Ti_{14}\}$ layer $\{Ti@Ti_5\}$ pentagons can be identified, which act as the building blocks of the recently constructed fullerene-like $\{Ti_{42}\}$ cluster.[30] The $\{Ti_{52}O_{74}\}$ cluster core of **COM-3** possess a large outside diameter of 4.0 nm (carbon and hydrogen atoms are not included) and an inside diameter of 3.6 nm (taking off the ionic radius of two Ti^{4+} ions), which is four times larger than **COM-1** and **COM-2**. Such a large $\{Ti_{52}O_{74}\}$ cluster core can even be directly visualized by high-resolution TEM (Figure S25). Moreover, from the view of nuclearity, **COM-3** is 10 atoms greater than the formerly largest $\{Ti_{42}\}$; while from the view of diameter, the size of **COM-3** is nearly twice as much as that of the Ti_{34} and Ti_{42} cluster (Figure S18).[14]

The stability of **COM-1** and **COM-3** were studied by treating their crystalline samples in acidic and alkaline aqueous solutions for 24 h. PXRD analysis confirms that both of them were stable between pH 3 and 13 (Figures S31 and S32). Their high chemical stabilities should be due to the protection effect of organic ligands.

Diffuse reflectance spectroscopy was used to study the ultraviolet−visible absorption of **COM-1** and **COM-3** (Figure 4). $BaSO_4$ was used as a blank, and absorbance was expressed

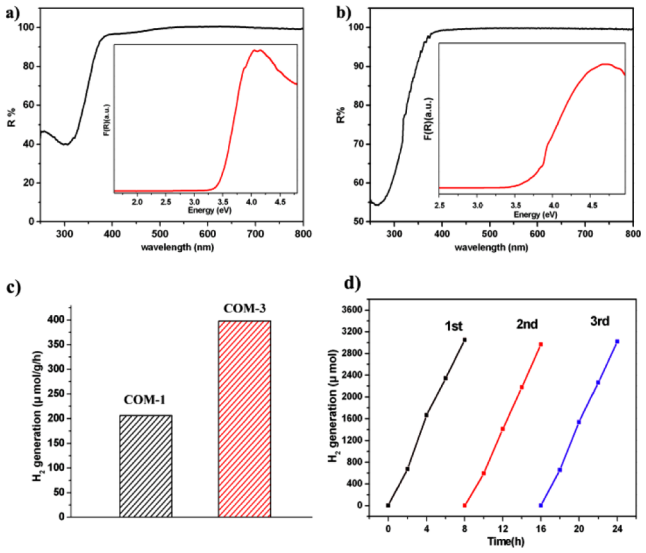

Figure 4. Optical and photocatalytic properties of **COM-1** and **COM-3**. (a) The solid-state ultraviolet−visible diffuse reflectance spectrum of **COM-1**, with the bandgap calculated to be 3.46 eV (insert). (b) The solid-state ultraviolet−visible diffuse reflectance spectrum of **COM-3**, with the bandgap calculated to be 3.69 eV (insert). (c) The comparison of the H_2 production rates of **COM-1** and **COM-3**. (d) Recycling water-splitting H_2 evolution tests under UV−visible light illumination on **COM-3**.

by treating the reflectance data with the Kubelka−Munk function.[31] According to the UV absorption edges of 358 and 336 nm, the bandgaps of **COM-1** and **COM-3** were experimentally estimated to be 3.46 and 3.69 eV, respectively. The slightly smaller bandgap of **COM-1** might be attributed to the existence of 1,2-benzenedicarboxylic ligands in its structure. The TiO_2 nanoparticles show an absorption edge around 390 nm, corresponding to a bandgap of about 3.2 eV.[32] Therefore, the absorption edges of **COM-1** and **COM-3** shift toward shorter wavelength in comparison with bulk TiO_2. Such blue-shift is likely the result of the different bonding within the titanium oxide core and also the incorporation of alkoxide and propionic groups.

UV light-driven water-splitting H_2 production studies were carried out using crystalline samples of **COM-1** and **COM-3** as photocatalysts and methanol as a sacrificial reducing agent. The evolved hydrogen was monitored by online gas chromatography (GC) analysis. Sampling was performed at an interval of 2 h over 8 h during the reaction. For both catalysts, the experimental results showed linear increase of the amount of produced H_2 during the entire testing period. Interestingly, although **COM-1** and **COM-3** represent similar bandgaps, their photocatalytic activities differ significantly from each other. The H_2 production rates for **COM-1** and **COM-3** are 206 and 398 μmol/h/g, respectively (Figure 4c). Therefore, by growing the cluster nuclearity from 6 to 52, the H_2 evolution activity has increased by almost 100%, giving rise to the highest H_2 production rate reported for TOCs. Moreover, the recycling experiments reveal that there is no obvious reduction of photocatalytic activity after three cycles for both **COM-1** (Figure S22) and **COM-3** (Figure 4d), indicating good photocatalysis stability of these materials.

In summary, we successfully developed a crystal growth approach to make atomically precise titanium−oxo clusters larger and larger. A stepwise assembly strategy has been applied to construct a 3.6 nm Ti_{52}−oxo cluster with boat-like interlayer structure (**COM-3**). So far **COM-3** holds two new records in the family of TOCs: largest size and highest efficiency for photocatalytic H_2 production. Photocatalytic water-splitting H_2 evolution studies confirm that both the Ti_6 and Ti_{52}−oxo clusters are efficient and stable catalysts; while the H_2 production rate of the latter is twice as much as that of the former, indicating interesting cluster size-effect. The success of our work provides a significant advancement in the construction of large Ti−oxo nanoclusters that can be comparable with TiO_2 nanoparticles. Moreover, our investigation on the influence of connectivity and nuclearity on the photocatalytic activities of TOCs will benefit a lot for the understanding of the structure−property relationships of titanium oxide nanoparticles.

■ ASSOCIATED CONTENT

Supporting Information

The Supporting Information is available free of charge on the ACS Publications website at DOI: 10.1021/jacs.6b03489.

Synthesis, EDS, IR, TGA curve, PXRD data, ESI−MS spectra, and detailed structure analysis (PDF)

■ AUTHOR INFORMATION

Corresponding Authors

*lzhang@fjirsm.ac.cn
*zhj@fjirsm.ac.cn

Notes

The authors declare no competing financial interest.

The X-ray crystallographic coordinates for structures reported in this article have been deposited at the Cambridge Crystallographic Data Centre (CCDC) under deposition numbers CCDC 1469737 (**COM-1**), CCDC 1469738 (**COM-2**), and CCDC 1454994 (**COM-3**). These data can be obtained free of charge from the Cambridge Crystallographic Data Centre via http://www.ccdc.cam.ac.uk/data_request/cif

DOI: 10.1021/jacs.6b03489
J. Am. Chem. Soc. 2016, 138, 7480−7483

■ ACKNOWLEDGMENTS

Research reported in this publication was supported by the Strategic Priority Research Program of the Chinese Academy of Sciences (Grant No. XDB20000000), the 973 program (2012CB821705) and NSFC (21425102, 21401191, 21521061, and 21501176).

■ REFERENCES

(1) Kudo, A.; Miseki, Y. *Chem. Soc. Rev.* **2009**, *38*, 253−278.
(2) Sun, Z.; Zheng, H.; Li, J.; Du, P. *Energy Environ. Sci.* **2015**, *8*, 2668−2676.
(3) Tachibana, Y.; Vayssieres, L.; Durrant, J. R. *Nat. Photonics* **2012**, *6*, 511−518.
(4) Kubacka, A.; Fernandez-Garcia, M.; Colon, G. *Chem. Rev.* **2012**, *112*, 1555−1614.
(5) Yang, H. G.; Liu, G.; Qiao, S. Z.; Sun, C. H.; Jin, Y. G.; Smith, S. C.; Zou, J.; Cheng, H. M.; Lu, G. Q. *J. Am. Chem. Soc.* **2009**, *131*, 4078−4083.
(6) Tan, H.; Zhao, Z.; Niu, M.; Mao, C.; Cao, D.; Cheng, D.; Feng, P.; Sun, Z. *Nanoscale* **2014**, *6*, 10216−10223.
(7) Zuo, F.; Bozhilov, K.; Dillon, R. J.; Wang, L.; Smith, P.; Zhao, X.; Bardeen, C.; Feng, P. *Angew. Chem., Int. Ed.* **2012**, *51*, 6223−6226.
(8) Zhao, Z.; Zhang, X. Y.; Zhang, G. Q.; Liu, Z. Y.; Qu, D.; Miao, X.; Feng, P. Y.; Sun, Z. C. *Nano Res.* **2015**, *8*, 4061−4071.
(9) Coppens, P.; Chen, Y.; Trzop, E. *Chem. Rev.* **2014**, *114*, 9645−9661.
(10) Rozes, L.; Sanchez, C. *Chem. Soc. Rev.* **2011**, *40*, 1006−10030.
(11) Matthews, P. D.; King, T. C.; Wright, D. S. *Chem. Commun.* **2014**, *50*, 12815−12823.
(12) Czakler, M.; Artner, C.; Schubert, U. *Eur. J. Inorg. Chem.* **2014**, *2014*, 2038−2045.
(13) Watenpaugh, K.; Caughlan, C. N. *Chem. Commun.* **1967**, 76−77.
(14) Sokolow, J. D.; Trzop, E.; Chen, Y.; Tang, J.; Allen, L. J.; Crabtree, R. H.; Benedict, J. B.; Coppens, P. *J. Am. Chem. Soc.* **2012**, *134*, 11695−11700.
(15) Lv, Y.; Cheng, J.; Steiner, A.; Gan, L.; Wright, D. S. *Angew. Chem., Int. Ed.* **2014**, *53*, 1934−1938.
(16) Lv, Y.; Willkomm, J.; Steiner, A.; Gan, L.; Reisner, E.; Wright, D. S. *Chem. Sci.* **2012**, *3*, 2470−2473.
(17) Snoeberger, R. C.; Young, K. J.; Tang, J. J.; Allen, L. J.; Crabtree, R. H.; Brudvig, G. W.; Coppens, P.; Victor, S. B.; Benedict, J. B. *J. Am. Chem. Soc.* **2012**, *134*, 8911−8917.
(18) Negre, C. F. A.; Young, K. J.; Oviedo, M. B.; Allen, L. J.; Sanchez, C. G.; Jarzembska, K. N.; Benedict, J. B.; Crabtree, R. H.; Coppens, P.; Brudvig, G. W.; Batista, V. S. *J. Am. Chem. Soc.* **2014**, *136*, 16420−16429.
(19) Benedict, J. B.; Freindorf, R.; Trzop, E.; Cogswell, J.; Coppens, P. *J. Am. Chem. Soc.* **2010**, *132*, 13669−13671.
(20) Chen, Y.; Trzop, E.; Sokolow, J. D.; Coppens, P. *Chem. - Eur. J.* **2013**, *19*, 16651−16655.
(21) Fornasieri, G.; Rozes, L.; Le Calve, S.; Alonso, B.; Massiot, D.; Rager, M. N.; Evain, M.; Boubekeur, K.; Sanchez, C. *J. Am. Chem. Soc.* **2005**, *127*, 4869−4878.
(22) Hou, J. L.; Luo, W.; Wu, Y. Y.; Su, H. C.; Zhang, G. L.; Zhu, Q. Y.; Dai, J. *Dalton Trans.* **2015**, *44*, 19829−19835.
(23) Day, V. W.; Eberspacher, T. A.; Klemperer, W. G.; Park, C. W. *J. Am. Chem. Soc.* **1993**, *115*, 8469−8470.
(24) Chaumont, C.; Mobian, P.; Henry, M. *Dalton Trans.* **2014**, *43*, 3416−3419.
(25) Wu, Y. Y.; Lu, X. W.; Qi, M.; Su, H. C.; Zhao, X. W.; Zhu, Q. Y.; Dai, J. *Inorg. Chem.* **2014**, *53*, 7233−7240.
(26) Liu, Z.; Lei, J.; Frasconi, M.; Li, X.; Cao, D.; Zhu, Z.; Schneebeli, S. T.; Schatz, G. C.; Stoddart, J. F. *Angew. Chem., Int. Ed.* **2014**, *53*, 9193−9197.
(27) Corden, J. P.; Errington, W.; Moore, P.; Partridge, M. G.; Wallbridge, M. G. H. *Dalton Trans.* **2004**, 1846−1851.
(28) Lin, Y.; Zhu, Y.-F.; Chen, Z.-H.; Liu, F.-H.; Zhao, L.; Su, Z.-M. *Inorg. Chem. Commun.* **2014**, *40*, 22−25.
(29) Liu, J.-X.; Gao, M.-Y.; Fang, W.-H.; Zhang, L.; Zhang, J. *Angew. Chem., Int. Ed.* **2016**, *55*, 5160−5165.
(30) Gao, M.-Y.; Wang, F.; Gu, Z.-G.; Zhang, D.-X.; Zhang, L.; Zhang, J. *J. Am. Chem. Soc.* **2016**, *138*, 2556−2559.
(31) Wendlandt, W. W.; Hecht, H. G. *Reflectance Spectroscopy*; Interscience Publishers: New York, 1966.
(32) Scanlon, D. O.; Dunnill, C. W.; Buckeridge, J.; Shevlin, S. A.; Logsdail, A. J.; Woodley, S. M.; Catlow, C. R.; Powell, M. J.; Palgrave, R. G.; Parkin, I. P.; Watson, G. W.; Keal, T. W.; Sherwood, P.; Walsh, A.; Sokol, A. A. *Nat. Mater.* **2013**, *12*, 798−801.

DOI: 10.1021/jacs.6b03489
J. Am. Chem. Soc. 2016, 138, 7480−7483